

Supporting Information:

From starphenes to non-benzenoid linear conjugated polymers by substrate templating

Mohammed S. G. Mohammed^{1,2,‡}, James Lawrence^{1,2,‡,}, Fátima García³, Pedro Brandimarte¹, Alejandro Berdonces-Layunta^{1,2}, Dolores Pérez,³ Daniel Sánchez-Portal,^{1,2} Diego Peña^{3,*} and Dimas G. de Oteyza^{1,2,4,*}*

1. Donostia International Physics Center (DIPC), San Sebastián, Spain.
2. Centro de Física de Materiales-Material Physics Center (CFM-PCM), San Sebastián, Spain.
3. Centro Singular de Investigación en Química Biolóxica e Materiais Moleculares (CiQUS) and Departamento de Química Orgánica, Universidade de Santiago de Compostela, Santiago de Compostela, Spain.
4. Ikerbasque, Basque Foundation for Science, Bilbao, Spain.

[‡] These Authors contributed equally to this work.

Corresponding Author: * james.lawrence@dipc.org, * diego.pena@usc.es, * d_g_oteyza@ehu.eus

Contents:

1. Methods
 - 1.1. Synthesis of precursor molecule **m1**
 - 1.2. NMR spectra
 - 1.3. Sample preparation
 - 1.4. STM imaging
 - 1.5. DFT calculations
2. Additional figures
3. References

1. Methods

1.1 Synthesis of precursor molecule m1

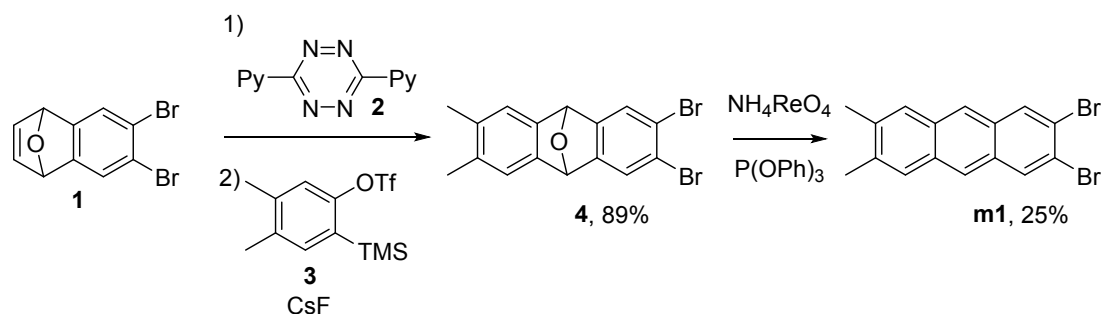
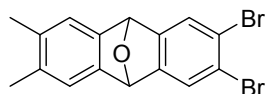


Figure S1. Synthetic route to obtain compound **m1** by solution chemistry.

Dibromoepoxinaphthalene **1**^[1] and triflate **3**^[2] were synthesized according to reported procedures, showing the same spectroscopically properties as those reported.

1.1.1 Synthesis of epoxianthracene **4**



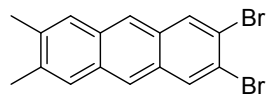
6,7-Dibromo-1,4-dihydro-1,4-epoxinaphthalene (1.57 g, 4.64 mmol) and 3,6-di(pyridin-2-yl)-1,2,4,5-tetrazine (1.09 g, 4.64 mmol) were dissolved in dry dichloromethane (25 mL) and heated at 42°C for 1.5 h. The reaction mixture was allowed to reach room temperature and then it was diluted with dry acetonitrile (25 mL). Then, triflate **3** was added in dichloromethane solution (4 mL) followed by the addition of caesium fluoride (3.50 g, 23.6 mmol). The reaction was heated at 42°C overnight. Then, the solvents were evaporated, the residue was dissolved in dichloromethane (20 mL) and washed with sodium bicarbonate saturated aqueous solution (2×10 mL). The crude was purified by column chromatography (silica gel, hexane: ethyl acetate 1:1) yielding epoxianthracene **4** as a white solid (0.80 g, 89% yield).

¹H NMR (300 MHz, CDCl₃, 25°C) δ 7.52 (2H, s), 7.12 (2H, s), 5.95 (2H, s), 2.19 (6H, s) ppm.

¹³C NMR (75 MHz, CDCl₃, 25°C) δ 149.65 (C Ar), 144.53 (C Ar), 134.57 (C Ar), 125.41 (CH Ar), 122.30 (CH Ar), 121.43 (C Ar), 81.94 (CH-O), 19.94 (CH₃) ppm.

HRMS (APCI): for C₁₆H₁₃Br₂O calculated: 378.9328, observed 378.9326.

1.1.2 Synthesis of 2,3-dibromo-7,8-dimethylantracene (**m1**)



Epoxianthracene **4** (86 mg, 0.226 mmol), triphenylphosphite (84 mg, 0.272 mmol) and ammonium perrhenate (2 mg, 0.06 mmol) were dissolved in 3 mL of toluene. The reaction mixture was heated at 80°C for 24 hours. The reaction mixture was allowed to reach room temperature. Then, the precipitate was sequentially washed and the suspensions centrifugated (6000 rpm, 5 min) with: 1X diethyl ether, 1X dichloromethane, 2X chloroform yielding 2,3-dibromo-7,8-dimethylantracene (**m1**) as a light yellowish solid (21 mg, 25%).

¹H NMR (300 MHz, C₂D₂Cl₄, 90°C) δ 8.32 (s, 2H), 8.21 (s, 2H), 7.77 (s, 2H), 2.52 (s, 6H) ppm.

¹³C NMR (126 MHz, C₂D₂Cl₄, 90°C) δ 136.73 (C Ar), 132.02 (CH Ar), 131.66 (C Ar), 130.41 (C Ar), 126.86 (CH Ar), 123.93 (CH Ar), 120.58 (C Ar), 20.00 (CH₃) ppm.

HRMS (APCI): for C₁₆H₁₃Br₂ [M+H]⁺ calculated: 362.9379, observed 362.9376.

1.2. NMR spectra

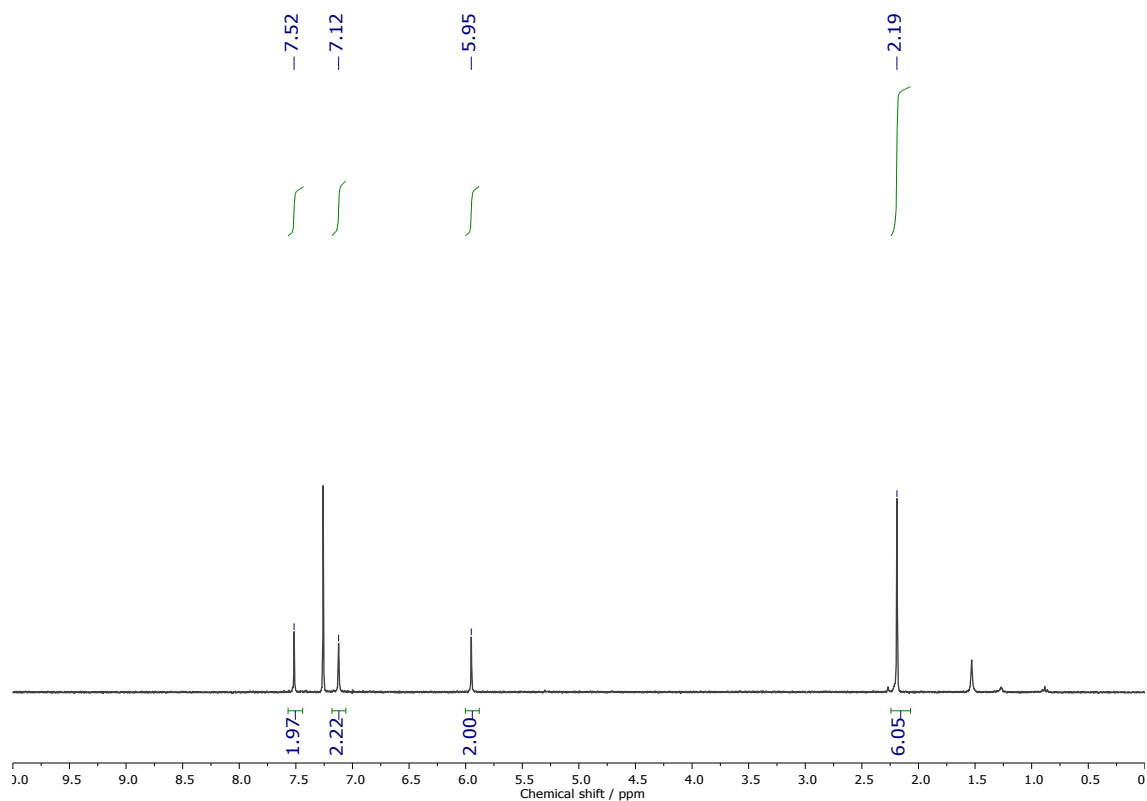


Figure S2. ^1H NMR (300 MHz, CDCl_3 , 25°C) of epoxianthracene **4**.

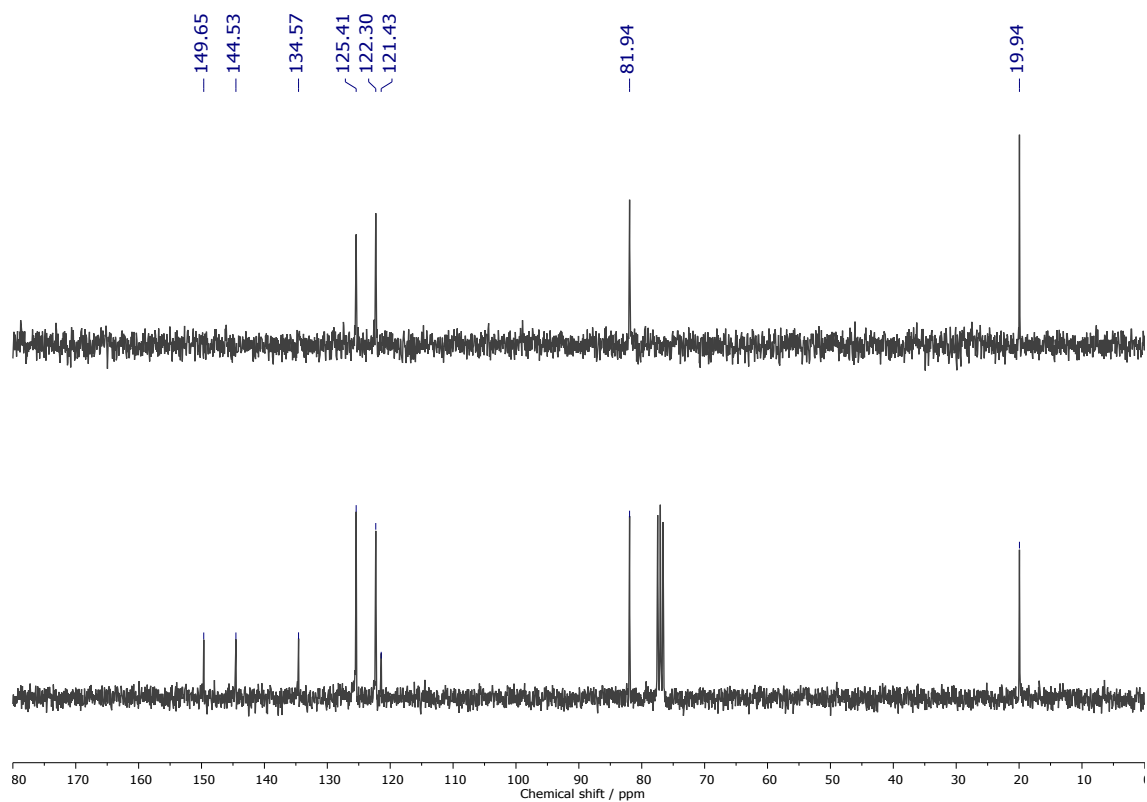


Figure S3. DEPT-135 (top) and ^{13}C NMR (75 MHz, CDCl_3 , 25°C) of epoxianthracene **4**.

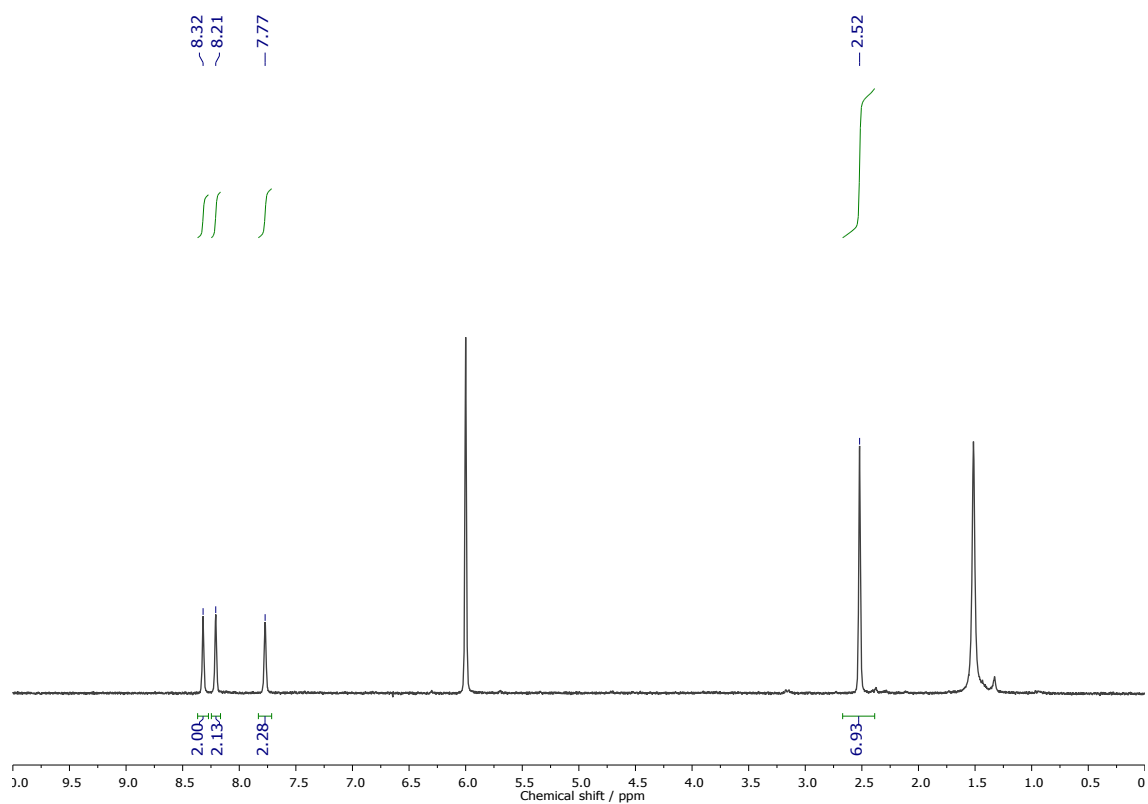


Figure S4. ^1H NMR (300 MHz, $\text{C}_2\text{D}_2\text{Cl}_4$, 90°C) of 2,3-dibromo-7,8-dimethylantracene (**m1**).

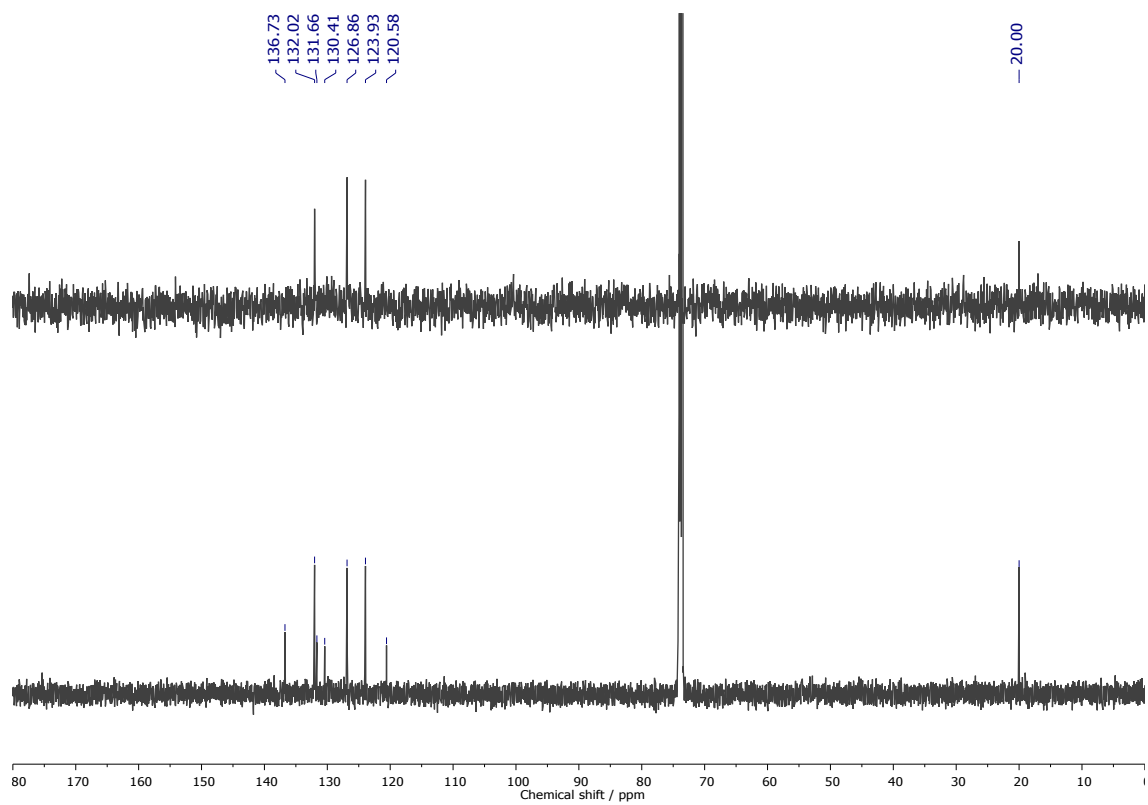


Figure S5. DEPT135 (top) and ^{13}C NMR (126 MHz, $\text{C}_2\text{D}_2\text{Cl}_4$, 90°C) of 2,3-dibromo-7,8-dimethylantracene (**m1**).

1.3 Sample preparation.

The Au(111) single crystal was cleaned by multiple cycles of Ar⁺ sputtering (1 KeV, 4 E-6 mbar, 20 μ A for 30 minutes) and flash annealing to 750 K. Functionalized anthracene precursor molecules **m1** were sublimed from a custom-built Knudsen cell evaporator at 385 K with the Au(111) surface held at room temperature. The sample was subsequently annealed to 425 K and 525 K.

The Au(110) single crystal was cleaned by applying sputtering conditions that were similar to those of Au(111) but with a lower annealing temperature of 575 K to maintain the homogeneous 2 \times 1 surface reconstruction. Similar precursor sublimation conditions were used. The sample was then annealed to 525 K and 560 K in two separate preparations.

NaCl was deposited on each of the Au(111) and Au(110) samples via sublimation at 780 K. CO was then deposited on the various samples at similar dosing conditions: a sample base temperature of 4.3 K, a partial CO pressure of 9.0 E-9 mbar in the STM chamber, and a sample temperature maximum of 7.1 K with the STM thermal shields open during the dosage. The total CO deposition time was 80 seconds for each sample.

1.4 STM imaging.

All the experimental results were acquired using a commercial low-temperature scanning tunneling microscope (Scientia-Omicron) operating under ultra-high-vacuum (UHV) conditions. The base pressure for measurements was below 1E-10 mbar with a sample temperature of 4.3 K. Cl-functionalization of the tip was performed on Au(111) following the procedure as described by Lawrence et al.^[3] On Au(110) Cl-terminated tips were achieved similarly by approaching the STM metal tip over an NaCl island by 420 pm from starting feedback parameters of 20 mV/100 pA. A clear enhancement of the imaging resolution and the appearance of a “hole-like” trace at the missing Cl position evidence the Cl-functionalization (Figure S6). dI/dV measurements were performed using a lock-in modulator with an oscillation frequency of 827 Hz and amplitude of 20-30 mV. STM images were analyzed using WSxM.^[4]

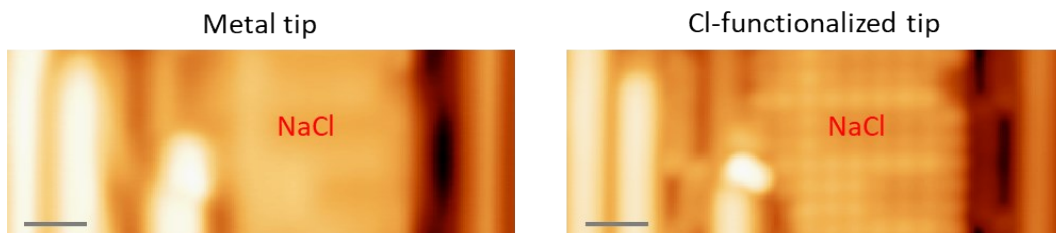


Figure S6. STM topography images comparing the imaging resolution of a region on the Au(110) sample with a metallic tip and with a Cl-terminated tip. Images are scanned at 100 mV/100 pA and scale bar is 1 nm for both images.

1.5 DFT calculations.

Density Functional Theory simulations were performed with the SIESTA package.^[5-7] We used the van der Waals density functional by Dion et al,^[8] with the modified exchange correlation by Klimeš, Bowler and Michaelides.^[9] The valence-electron wave functions are expanded using a double- ζ plus polarization (DZP) basis set with the orbital radii extension defined using a 30 meV energy shift,^[6] while the core electrons were replaced by norm-

conserving Troullier-Martins pseudopotentials.^[10] The fineness of the real space grid used for integration was defined by setting an energy cutoff of 300 Ry.^[6] The smearing of the electronic occupations was determined using a Fermi-Dirac distribution, and 300 K of electronic temperature. Self-consistency was considered to be achieved when the changes of the density matrix elements were smaller than 10^{-6} as well as smaller than 10^{-5} eV for the Hamiltonian matrix elements. We used periodic boundary conditions with sufficiently large unit cells (at least 20 Å of vacuum space along all directions was used for determining the simulation cell for all systems, in order to avoid interaction between replicas in neighbouring cells). Geometry optimizations were performed using the conjugate gradient method until all forces were lower than 10 meV/Å. Constant-height STM simulations were performed in the Tersoff-Hamann approximation^[11] using the local density of states, taken 4 Å above the molecular plane to account for the tip-sample distance and the locally different orbital decay into the vacuum. The STM post-processing tool distributed with SIESTA was used for an accurate extrapolation of the local density of states at such high distance over the molecular plane, avoiding spurious effects associated with the finite range of the numerical atomic orbitals used as a basis set.

2 Additional figures.

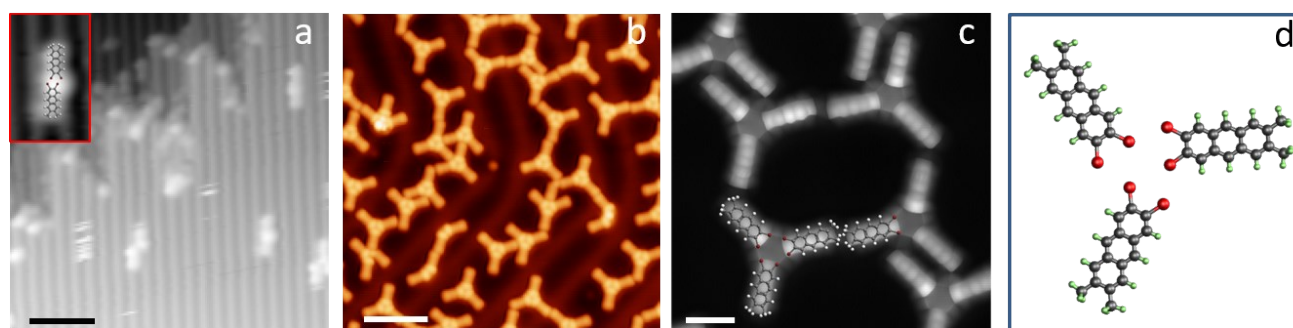


Figure S7. As deposited **m1** molecules: a) STM topography image of the precursor molecules on Au(110) with the molecular model in the inset, b) STM topography image for the molecules on Au(111) and c) constant height STM image with CO-functionalized tip for molecules on Au(111). d) Relaxed structure for a trimer of free-standing molecules. STM imaging parameters: a) -500 mV/70 pA, b) -500 mV/50 pA, c) 10 mV. Scale bar: a-b) 4 nm, c) 1 nm.

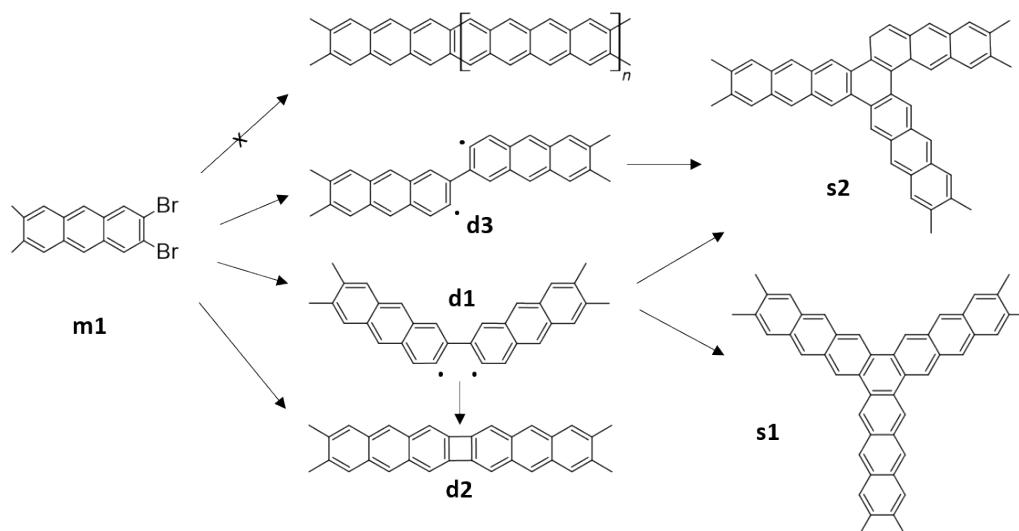


Figure S8. Possible reaction mechanisms for the five covalently bonded products on Au(111).

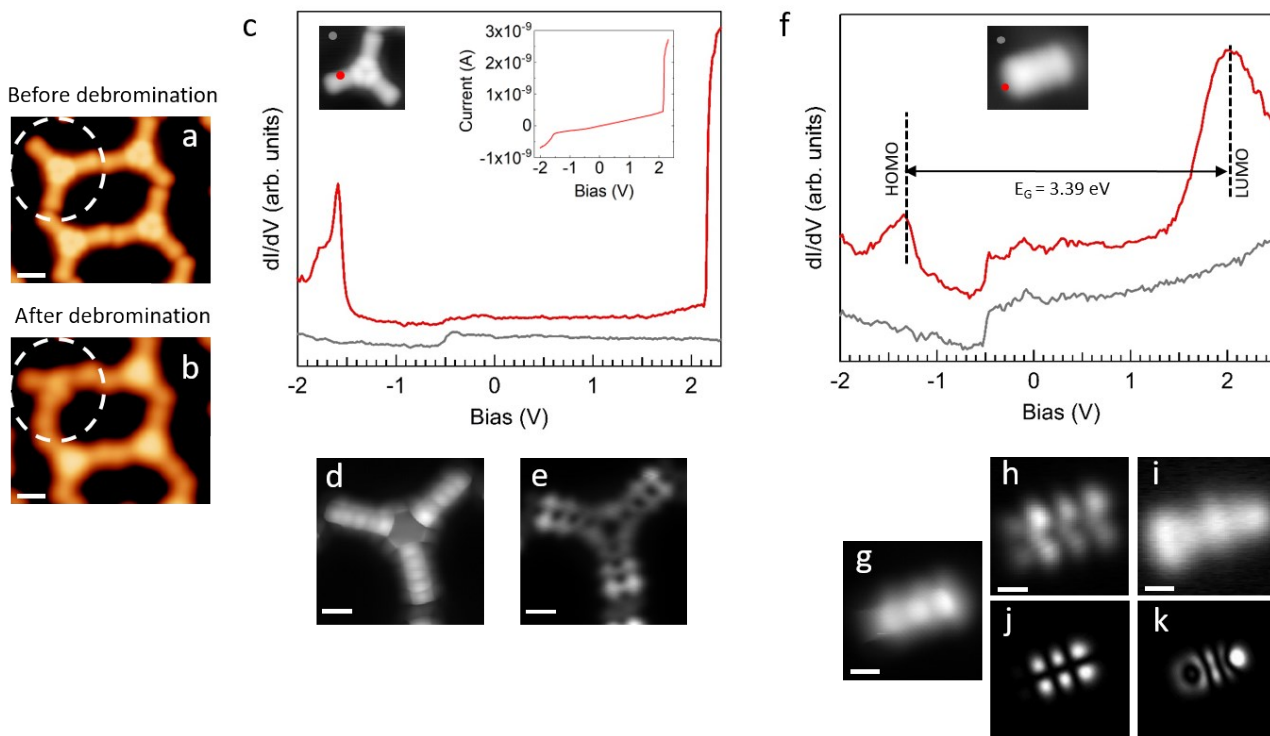


Figure S9. STM topography images of the monomer **m1** a) before and b) after tip-induced debromination. c) Differential conductance spectra on the brominated monomer and on the substrate (as reference) at the positions shown in the inset image. The inset curve is the corresponding current trace. d) Constant height STM image with CO-functionalized tip of a trimer consisting of halogen-assembled monomers. e) Corresponding constant-height dIdV map at its HOMO energy, namely -1.630 V. f) Differential conductance spectra of the monomer after debromination and of the substrate (as reference) at the positions shown in the inset image. g) Constant height image with CO-terminated tip of the debrominated monomer. Corresponding constant height dIdV maps at the energies of the h) HOMO (-1.340 V) and i) LUMO (2.050 V). Simulated STM images for the debrominated monomer **m1** at its j) HOMO and k) LUMO energy. STM imaging parameters: a) -0.520 V/50 pA,

b) -0.500 V/50 pA, d) 10 mV, g) 5 mV. Scale bar: a-b) 1 nm, d-e) 5 Å, g,h,j) 3 Å. In the calculations, the radicals left by debromination in **m1** have been saturated by H.

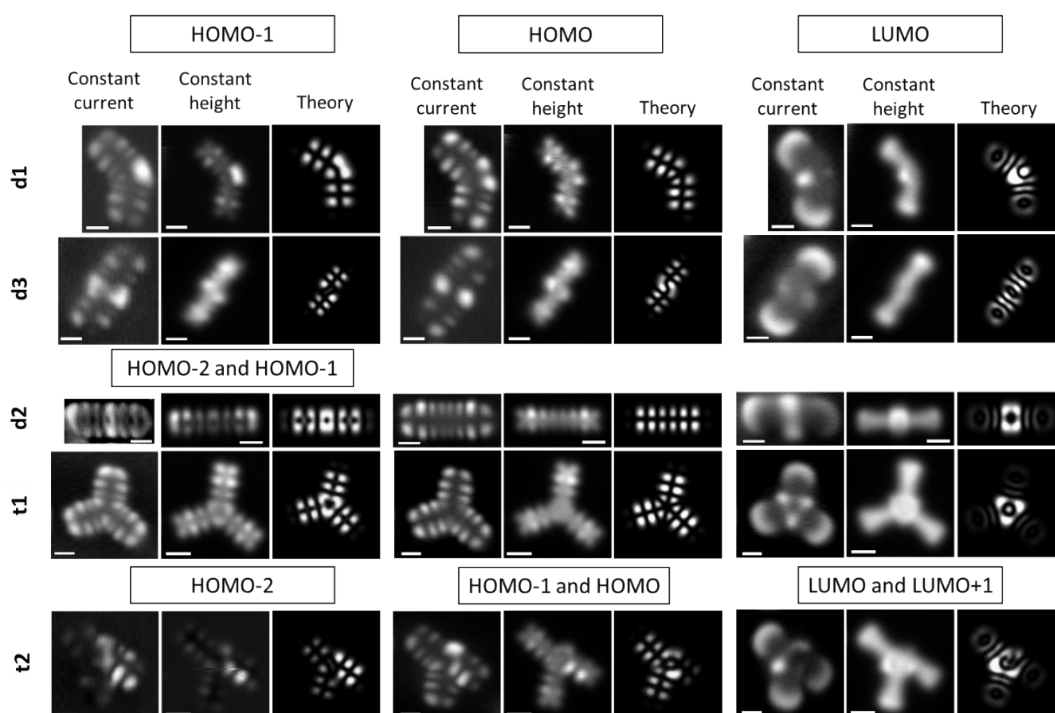


Figure S10. Constant height and constant current $dIdV$ maps of the observed low-energy resonances of molecular states associated to the five covalently bonded products on Au(111) comparing experimental data to theory (simulated at constant height) for each. Scale bar is 6 Å. The second occupied resonance for **d2** and **t1** corresponds to a convolution of the HOMO-1 and HOMO-2 orbitals that are quasi-degenerate and degenerate in the calculations, respectively. In turn, the first occupied and unoccupied resonances of **t2** correspond to a convolution of the quasi-degenerate HOMO and HOMO-1 for the former and of the quasi-degenerate LUMO and LUMO+1 for the latter. In the calculations, dangling bonds left by debromination in **d1** and **d3** have been saturated by H.

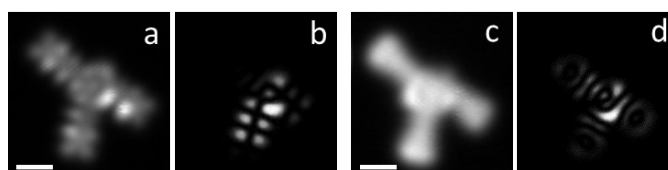


Figure S11. Constant height $dIdV$ maps of **t2** as compared to the calculated maps at the exact HOMO and LUMO energies: a) experimentally mapped HOMO, b) simulation at HOMO energy, c) experimentally mapped LUMO and d) simulation at LUMO energy. Scalebar is 6 Å for a and c.

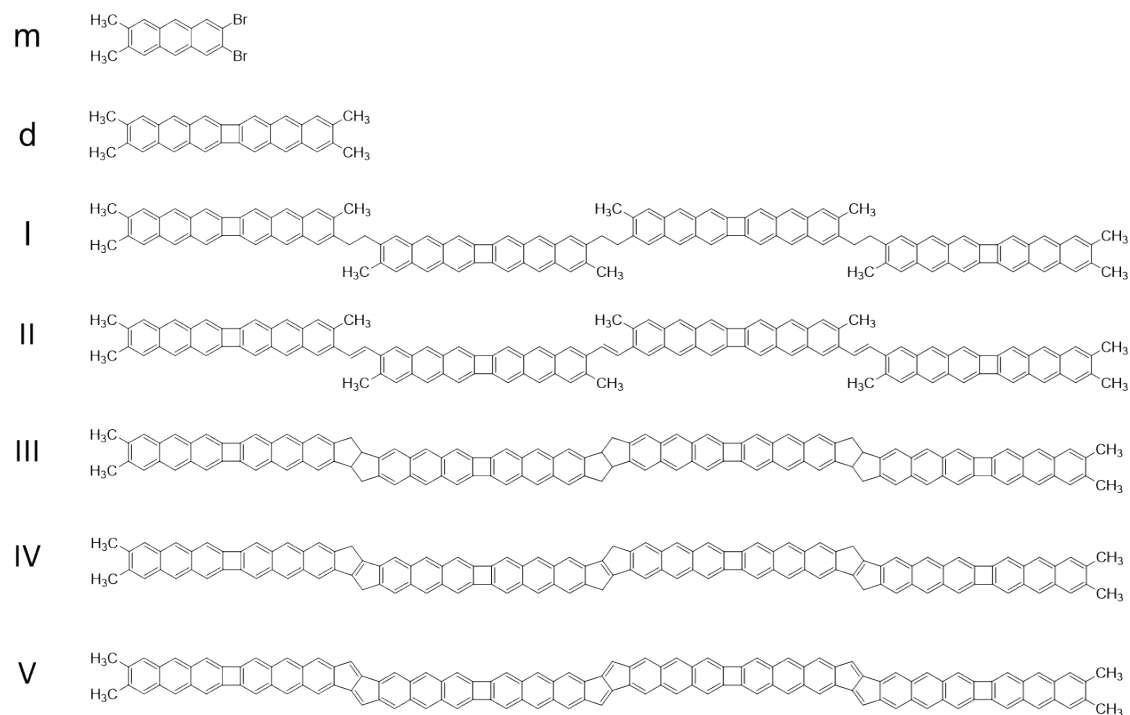


Figure S12. Chemical structure of the precursor molecule **m**), **d2** dimer **d**), I-V) possible coupling motifs of **d2**.

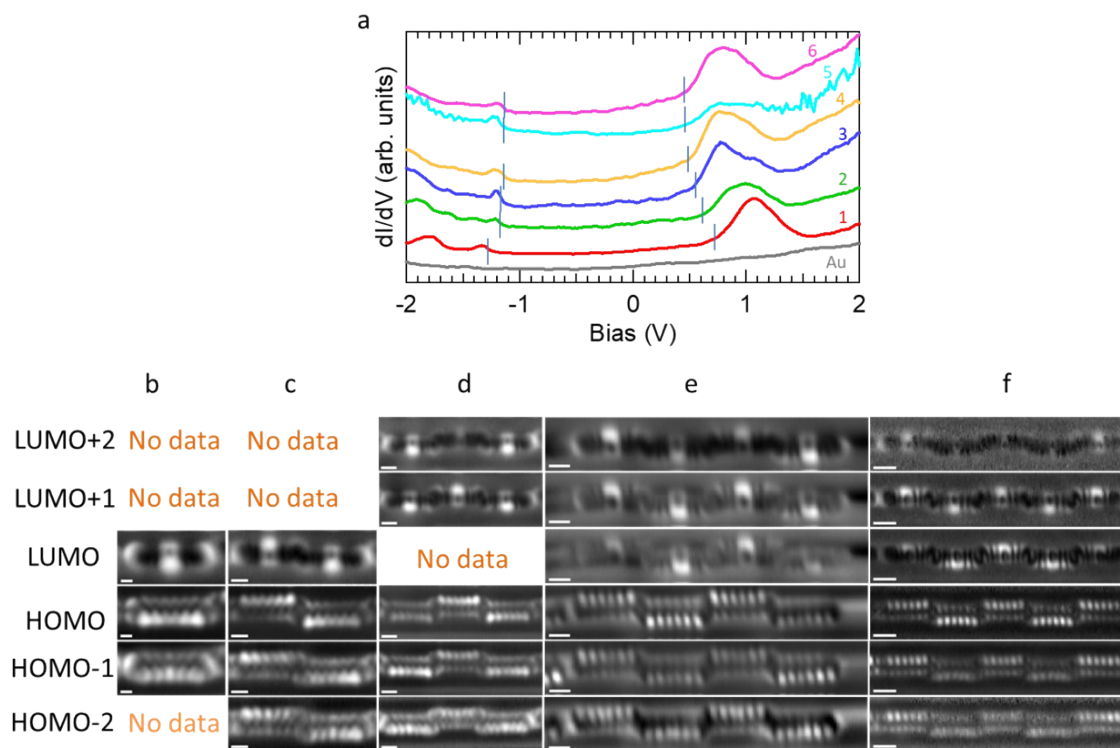


Figure S13. a) dI/dV point spectra of 1 to 6 conjugated dimer **d2** structures on Au(110), gray is the reference spectrum on the surface, vertical lines on each spectrum represent the onset of the frontier molecular orbitals. HOMO-2 to LUMO+2 constant current dI/dV mapping of b) monomer c) dimer d) trimer e) tetramer f) pentamer of conjugated **d2**. Scale bar b) 3 Å, c) 5 Å, d-e) 6 Å, f) 9 Å. All panels except e are imaged with a CO-functionalized tip. Panel e is instead recorded with a Cl tip.

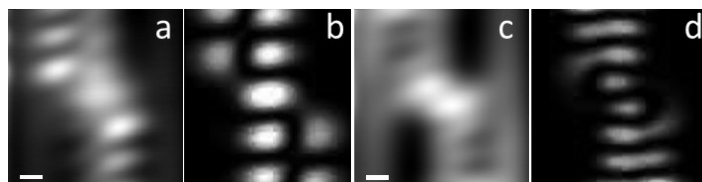


Figure S14. A close-up of constant height dIdV mapping at the junction between **d2** dimers. a) At the HOMO energy and b) the calculated HOMO map, c) at the LUMO energy and d) the calculated LUMO map. Constant height STM imaging parameters: a) -1.200 V, c) 0.650 V. Scale bar is 2 Å for a and c. The stronger intensity measured experimentally on the outer sides of the molecules, as compared with the stronger intensity predicted in the calculations, is well understood as the non-planar arrangement of the molecules within the Au(110) trenches that is not captured in the calculations. Calculations assume structure II in Fig. S6 for the junction.

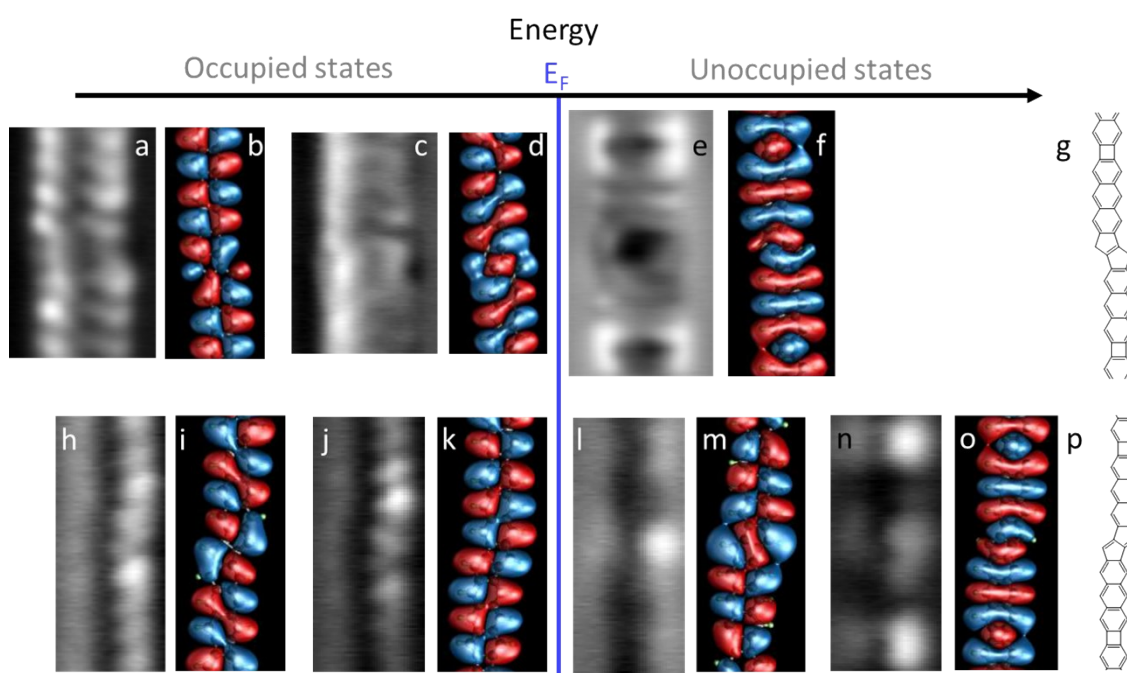


Figure S15. Constant current dIdV mapping of the polymers obtained after annealing to 560 K, a-f) showing the HOMO-1 to LUMO maps (in greyscale) with the associated wavefunction calculations for the structure in g), h-o) showing the HOMO-1 to LUMO+1 maps with the associated calculations for the structure in p).

3. References

- [1] R. Akita, K. Kawanishi, T. Hamura, *Org. Lett.* **2015**, *17*, 3094–3097.
- [2] A. Biju, F. Glorius, *Angewandte Chemie International Edition* **2010**, *49*, 9761–9764.
- [3] J. Lawrence, P. Brandimarte, A. Berdonces-Layunta, M. S. G. Mohammed, A. Grewal, C. C. Leon, D. Sánchez-Portal, D. G. de Oteyza, *ACS Nano* **2020**, *14*, 4499–4508.
- [4] I. Horcas, R. Fernández, J. M. Gómez-Rodríguez, J. Colchero, J. Gómez-Herrero, A. M. Baro, *Review of Scientific Instruments* **2007**, *78*, 013705.
- [5] E. Artacho, D. Sánchez-Portal, P. Ordejón, A. García, J. M. Soler, *Phys. Stat. Sol. B* **1999**, *215*, 809–817.

- [6] J. M. Soler, E. Artacho, J. D. Gale, A. García, J. Junquera, P. Ordejón, D. Sánchez-Portal, *Journal of Physics: Condensed Matter* **2002**, *14*, 2745–2779.
- [7] A. García, N. Papior, A. Akhtar, E. Artacho, V. Blum, E. Bosoni, P. Brandimarte, M. Brandbyge, J. I. Cerdá, F. Corsetti, R. Cuadrado, V. Dikan, J. Ferrer, J. Gale, P. García-Fernández, V. M. García-Suárez, S. García, G. Huhs, S. Illera, R. Korytár, P. Koval, I. Lebedeva, L. Lin, P. López-Tarifa, S. G. Mayo, S. Mohr, P. Ordejón, A. Postnikov, Y. Pouillon, M. Pruneda, R. Robles, D. Sánchez-Portal, J. M. Soler, R. Ullah, V. W. Yu, J. Junquera, *J. Chem. Phys.* **2020**, *152*, 204108.
- [8] M. Dion, H. Rydberg, E. Schröder, D. C. Langreth, B. I. Lundqvist, *Phys. Rev. Lett.* **2004**, *92*, 246401.
- [9] J. Klimeš, D. R. Bowler, A. Michaelides, *Journal of Physics: Condensed Matter* **2010**, *22*, 022201.
- [10] N. Troullier, J. L. Martins, *Phys. Rev. B* **1991**, *43*, 1993–2006.
- [11] J. Tersoff, D. R. Hamann, *Phys. Rev. Lett.* **1983**, *50*, 1998–2001.